Key Laboratory of Ministry of Education for Medicinal Plant Resources and Natural Pharmaceutical Chemistry, College of Life Sciences, Shaanxi Normal University, China

Comparison of protoporphyrin IX produced cell proliferation inhibition between human breast cancer MCF-7 and MDA-MB-231 cells

Long Li, Yan Chen, Xiaobing Wang, Xiaolan Feng, Pan Wang, Quanhong Liu

Received December 23, 2013, accepted January 25, 2014

Pan Wang & Quanhong Liu, Key Laboratory of Medicinal Resources and Natural Pharmaceutical Chemistry, Ministry of Education, National Engineering Laboratory for Resource Developing of Endangered Chinese Crude Drugs in Northwest of China, College of Life Sciences, Shaanxi Normal University, Shaanxi, Xi'an 710062, China. wangpan@snnu.edu.cn, lshaof@snnu.edu.cn

Pharmazie 69: 621–628 (2014) *doi: 10.1691/ph.2014.3985*

Protoporphyrin IX (PpIX) is an effective hematoporphyrin derivative, widely adopted in photodynamic therapy (PDT) and sonodynamic therapy (SDT). As a sensitizer, PpIX could significantly enhance laser light or ultrasound causing tumor cell damage in PDT/SDT studies. However, the biological function of PpIX itself has not been carefully defined. Recently, studies indicate that PpIX alone can inhibit Hela cell proliferation, but the potential mechanism was unclear. Therefore, in the present study it was investigated whether the proliferation inhibition effect generally occurred in human breast cancer MCF-7 and MDA-MB-231 cells. Different sensitivities and the involved mechanisms were carefully explored. Our results show that PpIX preferentially accumulated and selectively caused cell damage in human breast cancer MCF-7 and MDA-MB-231 cells compared with mouse embryonic fibroblast NIH-3T3. *In vitro*, PpIX induced cell viability decrease, intracellular ROS (reactive oxygen species) generation, and DNA damage in a concentration-dependent and cell-specific manner. MCF-7 was more sensitive to PpIX than MDA-MB-231 cells at the same PpIX dose. Western blots showed obvious enhancement of P53, and PUMA in a concentration dependent manner in MCF-7 cells, but not in MDA-MB-231 cells. In cell-free system, we also found that PpIX could interact with some large biological molecules, such as calf thymus DNA, and induce hyperchromic effects in spectroscopic analysis. Our findings imply that DNA might be one of the main targets of PpIX, and PpIX alone can cause significant tumor cell damage through ROS generation, while P53 status may play an important role in these processes.

1. Introduction

Protoporphyrin IX (PpIX) is known to be a hematoporphyrin derivative. Previous reports have shown that PpIX can accumulate specially in proliferative tumors (Ji et al. 2006), and has a high affinity to peripheral benzodiazepine receptors on the outer membrane of mitochondria (Pastorino et al. 1994). PpIX has been used as an effective sensitizer and was applied successfully in photodynamic therapy (PDT) and sonodynamic therapy (SDT) (Schneider-Yin et al. 2009; Chen et al. 2014; Su et al. 2014).

Recently, Bednarz et al. (2007) demonstrated that PpIX alone can induce HeLa cell apoptosis even without laser light or ultrasound excitation, suggesting that PpIX may have novelty function in tumor treatment. However, the actual mechanisms of PpIX for the toxic effect on tumor cells remain unclear. Here, we tried to investigate and compare the anti-tumor activity of PpIX in human breast cancer MCF-7 (wild-type p53) and MDA-MB-231 (mutant p53) cells, and also evaluated the potential mechanism.

In mammalian cells, tumor suppressor p53 plays important roles in a diversity of physiologic functions. Cellular p53 functions as a tumor suppressor by increasing genomic stability and inhibiting cell transformation (Bunz et al. 1998), initiating apoptosis upon defected DNA damage repair (Helton and Chen 2007; Fei and El-Deiry 2003). During stress, P53 rapidly translocates to the outer-membrane of mitochondria and engages with Bcl-2 family proteins, leading to permeabilization of the mitochondrial outermembrane, followed by the release of cytochrome c and initiation of apoptosis (Marchenko et al. 2000; Nemajerova et al. 2005). In addition, P53 can activate its downstream targets in a sequence specific manner to induce apoptosis. Several proapoptotic Bcl-2 family proteins, such as PUMA and Noxa, are shown to be critical mediators of p53-dependent apoptosis (Yu and Zhang 2005). However, mutations in the p53 tumor suppressor gene are observed in greater than 50 % of all human cancers (Hainaut and Hollstein 2000). Over 85 % of the mutations in the p53 gene are missense, rather than truncation or deletion mutants (Hainaut and Hollstein 2000; Hinds et al. 1990; Hollstein et al. 1991). So, these tumor derived p53 mutants are deficient in transcription activation as well as apoptosis induction.

In the present study, we investigated and compared PpIX induced cell viability loss, intracellular reactive oxygen species (ROS)

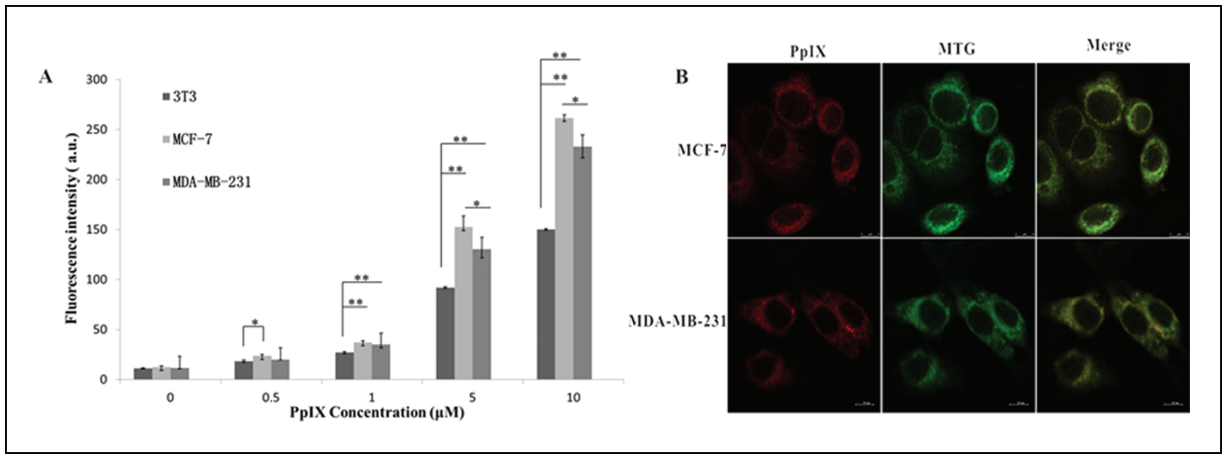

Fig. 1: PpIX preferential accumulation in breast cancer cells and its sub-cellular localization. (A) MCF-7, MDA-MB-231 and NIH-3T3 cells were treated with the indicated concentration of PpIX, the fluorescence intensity of intracellular PpIX was detected by flow cytometry. (B) Intracellular localization of PpIX in MCF-7 and MDA-MB-231 cells. After 2 h of incubation, PpIX displayed a red fluorescence pattern that corresponded well with that of the mitochondrial probe MTG (mitochondrion special dye). Data are means ± SE from three independent experiments. *$p < 0.05$, **$p < 0.01$ between groups.

production, DNA and nuclear damage, the protein and mRNA expression changes of p53 related genes in human breast cancer MCF-7 and MDA-MB-231 cells.

2. Investigations and results

2.1. PpIX preferential accumulated in breast cancer cells and its sub-cellular localization

In order to make sure PpIX preferential accumulation in tumors, we detected the intracellular PpIX levels in breast cancer cells MCF-7 and MDA-MB-231 and normal NIH-3T3 cells by flow cytometry under the same experimental conditions. The result (Fig. 1A) shows that, after 2 h incubation after PpIX adding, the fluorescence intensity of intracellular PpIX in breast cancer cells was obviously higher ($p < 0.01$) than that in NIH-3T3 cells when PpIX dose increased to 1 μM. When PpIX was 5 μM, the mean fluorescence intensity of intracellular PpIX in MCF-7 and MDA-MB-231 cells was 1.66 and 1.42 times greater than that in NIH-3T3 cells respectively. When PpIX was up to 10 μM, the intracellular PpIX level in three cell lines was all greatly increased, and the mean fluorescence intensity of intracellular PpIX in MCF-7 and MDA-MB-231 cells was 1.74 and 1.55 times greater than in NIH-3T3 cells. The PpIX level in MCF-7 was significantly higher than that in MDA-MB-231 cells when PpIX dose was 5 μM ($p < 0.05$) or 10 μM ($p < 0.05$).

The sub-cellular localization of PpIX may have great influence on subsequent cell damage. After 2 h incubation of PpIX, cells were co-loaded with MTG. The result (Fig. 1B) indicates the PpIX red fluorescence corresponded well with MTG green fluorescence, suggesting PpIX mainly accumulated in the mitochondria of MCF-7 and MDA-MB-231 cells.

2.2. Cell survival determination

Figure 2 shows that compared with non-treated control, the highest solvent group (DMSO alone) did not cause any cytotoxicity on MCF-7, MDA-MB-231 and NIH-3T3 cells. The PpIX treated cells would not produce any cytotoxic effect when its concentration was 0.5 μM, and produced significant cytotoxicity on MCF-7 when PpIX was 1 μM ($p < 0.05$). When the concentration of PpIX increased to 5 μM, it caused obvious cell viability loss both on MCF-7 ($p < 0.05$) and MDA-MB-231 ($p < 0.05$) cells. The cell viability was further decreased to 50.77 % ($p < 0.01$) and 62.99 % ($p < 0.05$) in MCF-7 and MDA-MB-231 cells, when PpIX dose was increased to 10 μM. When the concentration of PpIX increased from 1 μM to 10 μM, the cell viability of MCF-7 was very significantly decreased than MDA-MB-231 ($p < 0.01$). At the selected PpIX concentrations, PpIX did not cause any cytotoxic effect on NIH-3T3 cells.

2.3. ROS detection

PpIX mainly accumulated in the mitochondria of MCF-7 and MDA-MB-231 cells, so we next examined the mitochondria damage by detecting ROS generation. Mitochondria are the center of metabolism and the carrier of electron transfer chain, when mitochondria are destroyed, many free radicals such as O_2^- would be released and trigger cellular oxidative stress. In this study, we use a special dye–DCFH-DA being highly reactive with O_2^- to monitor intracellular ROS generation after PpIX treatment.

In Fig. 3, DCFH-DA combined with a fluorescence microscope detected that MCF-7 (Fig. 3A) and MDA-MB-231 (Fig. 3B) cells produced ROS under PpIX treatment. The green fluorescence intensity of DCF has positive correlation with the concentration of PpIX in MCF-7 and MDA-MB-231 cells, indicating that the ROS generation was closely related to the applied PpIX dose. In addition, the phase contrast images showed untreated MCF-7 cells spread very well and tightly attached on the coverslipe, while the PpIX treated cells was obviously shrunk, and partly floated from the coverslip when PpIX increased to 5 μM and 10 μM. Interestingly, the cells deformed seriously when they displayed bright DCF green fluorescence (as indicated by the white arrows), suggesting the ROS formation was a vital factor for causing MCF-7 cell damage after PpIX treatment. In MDA-MB-231 cells, a similar phenomenon was observed, but fewer cells showed severe deformation and ROS generation at the same PpIX treatment compared with MCF-7. The formed ROS in cells may have certain effects on DNA damage and mitochondrial damage.

2.4. DNA damage detection and nuclear morphological observation

Studies show that ROS are greatly related with DNA and subsequent cell damage (Collado et al. 2012). So we next examined nuclear DNA damage in MCF-7 and MDA-MB-231 cells by comet assay and DAPI staining. As shown in Fig. 4A, 2 h after PpIX-loading, PpIX caused serious DNA damage in different concentrations compared to the corresponding control either

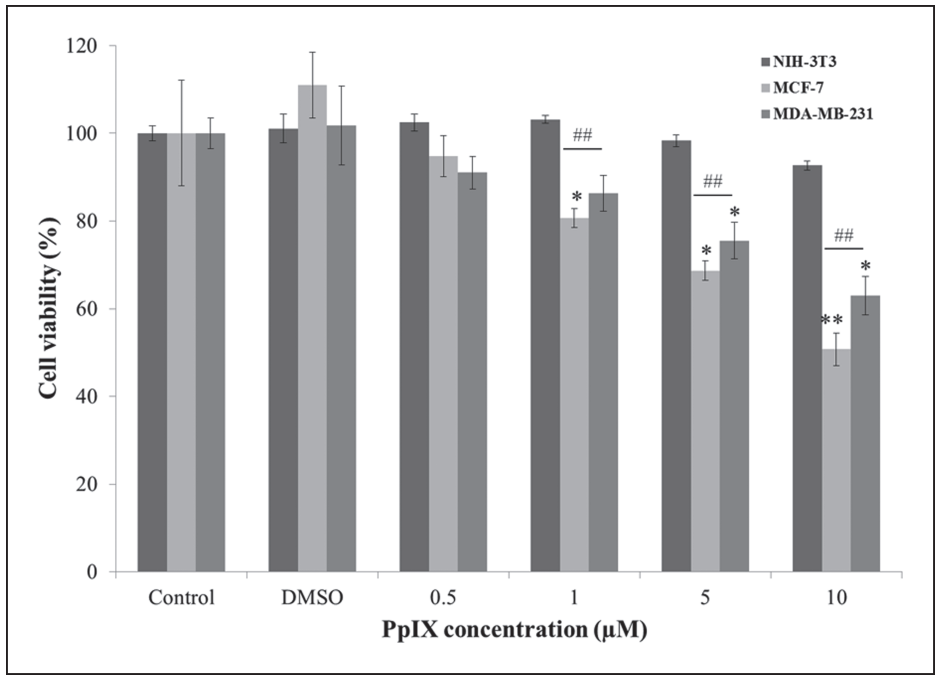

Fig. 2: Effects of different dose of PpIX on the viability of MCF-7, MDA-MB-231 and NIH-3T3 cells. Exponentially growing MCF-7, MDA-MB-231 and NIH-3T3 cells were treated with the indicated concentration of PpIX, cell viability was determined using the MTT assay after PpIX-loading. Data are means ± SE from three independent experiments. *$p < 0.05$, **$p < 0.01$ versus untreated controls. ##$p < 0.01$, between MCF-7 and MDA-MB-231 cells.

in MCF-7 or MDA-MB-231 cells. Analysis of the comet tail length (Fig. 4B) found that DNA damage for both cell lines were obviously PpIX-dose dependent. Even at the lowest PpIX dose, remarkable DNA damage was caused on both cells, suggesting that DNA damage was a sensitive and early marker for PpIX induced breast cancer cell damage. The PpIX caused DNA damage in MCF-7 cells was greatly higher than that in MDA-MB-231 cells at the same PpIX concentration ($p < 0.01$).

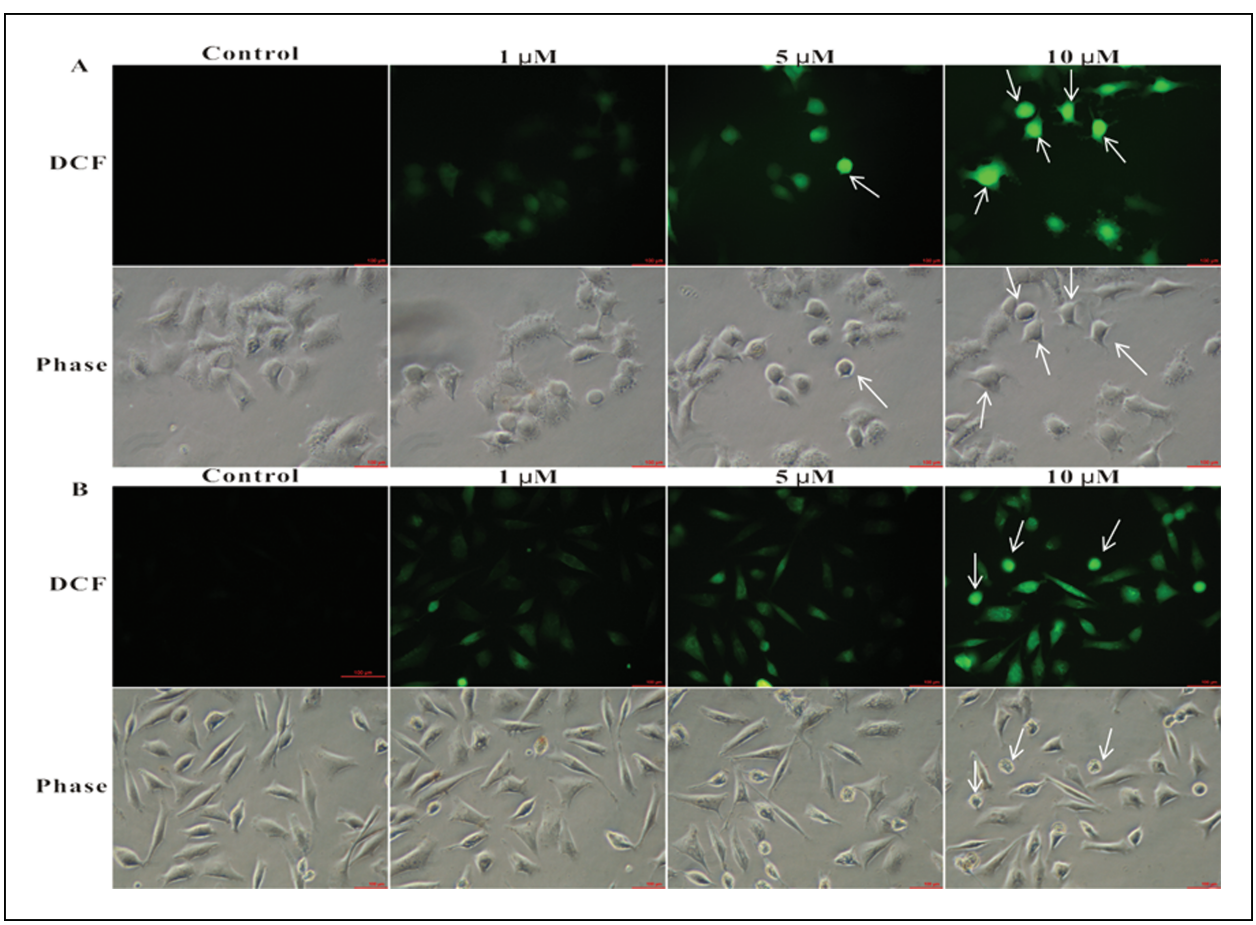

Fig. 3: Intracellular ROS generation in MCF-7 and MDA-MB-231 after PpIX treatment. DCFH-DA combined with fluorescence microscope showed PpIX treatment triggered intracellular ROS generation in MCF-7 (A) and MDA-MB-231 (B) cells. Bar = **.

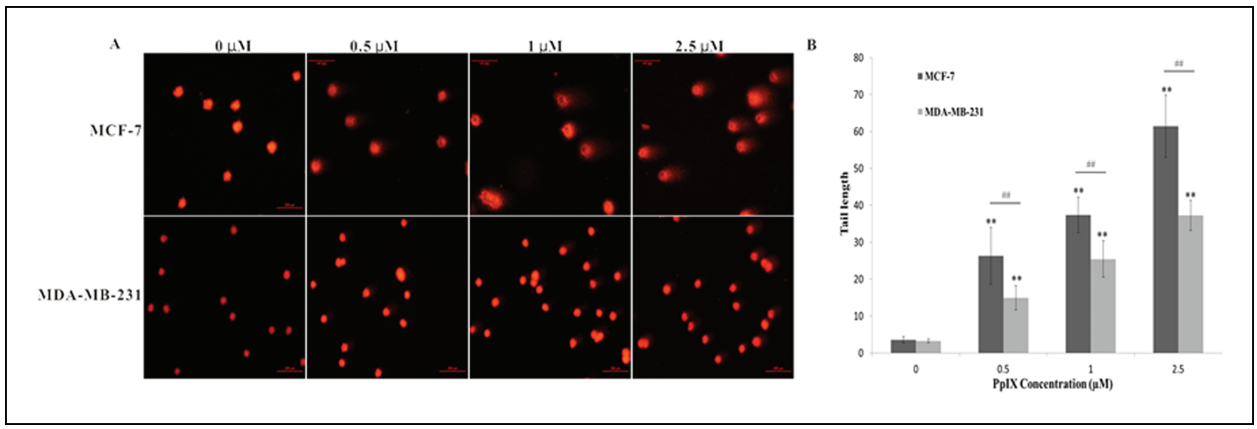

Fig. 4: DAPI staining was applied to observe the nuclear morphology change in MCF – 7 (A) and MDA-MB-231(B) cells.

The mean levels of comet tail length of MCF-7 were about 1.8 and 1.5 times than MDA-MB-231 when PpIX was 0.5 μM and 1 μM, and which increased to 1.7 times when PpIX increased to 2.5 μM. This result was very consistent with PpIX accumulation (Fig. 1A) and PpIX caused cytotoxicity (Fig. 2) in the two cell lines as shown above.

Six hours after treatment, control cells displayed a weak fluorescence and had no visible nuclear changes (Fig. 5). Both cell lines in the PpIX (1 μM) treated group showed enhancing DAPI staining, and few cells indicated damaged nuclei. In 5 μM and 10 μM groups, nuclear condensation with enhancing DAPI staining and altered nuclear morphology were more significant in MCF-7 and MDA-MB-231 cells.

2.5. PpIX induced calf thymus DNA damage in cell-free system

To further investigate PpIX caused DNA damage, we examined the interaction between PpIX and calf thymus DNA in cell-free system.

UV–Vis absorption measurement is a very simple method and applicable to explore the structural changes of DNA since it uses intrinsic fluorophores for investigation and avoid complicated labeling with an extrinsic dye under physiological conditions. DNA has a maximum absorption peak at the position about 260 nm, which is determined by the physical properties, and it will produce a hyperchromic effect if the structures change (Kurihara et al. 1963). Results in Fig. 6A show that 5 μM PpIX induced a hyperchromic effect compared to DNA alone, the fluorescence intensity at 260 nm increased regularly with the increasing concentration of DNA. When different concentrations of PpIX were added into 0.1 mg/ml DNA solution, the fluorescence intensity also increased with the increasing PpIX dose (Fig. 6B). These results indicate that PpIX alone could destroy the structure of DNA molecules *in vitro*.

2.6. Western blot analysis

Because DNA damage will stimulate P53 response, the next study was done to examine the expression levels of P53 and its downstream PUMA, Bcl-2 in MCF-7 and MDA-MB-231 cells after PpIX treatment. In MCF-7 cells, the expression levels of P53 and PUMA gradually increased in a PpIX-dependent manner, while Bcl-2 did not change (Fig. 7A). Incoordinately, in MDA-MB-231 cells, P53, PUMA and Bcl-2 all did not visibly change after PpIX treatment (Fig. 7B). This result indicated that P53 might be the key factor for the different PpIX induced cytotoxicity on human breast MCF-7 and MDA-MB-231 cells.

2.7. Reverse transcription-PCR

RT-PCR method was applied to detect the mRNA expression of p53 in MCF-7 and MDA-MB-231 cells after PpIX treatment. In MCF-7 cells, the mRNA expression of p53 increased significantly after PpIX treatment, this result was in agreement with the P53 protein expression by western blotting. In MDA-MB-231 cells, the mRNA expression of p53 did not significantly change

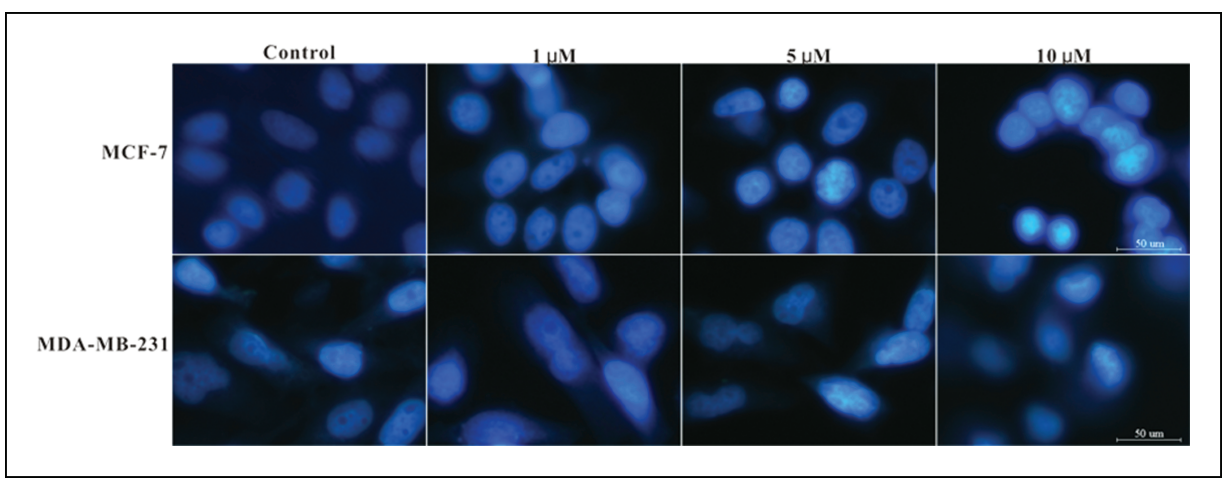

Fig. 5: DNA damage of MCF-7 and MDA-MB-231 cells after PpIX treatment. The DNA damage was detected by single cell gel eletrophoresis when MCF-7 and MDA-MB-231 cells were loaded with different does of PpIX, and visualized under fluorescent microscope (A). The obtained images were then analyzed with tail length by CASP software (B). At least 50 cells were analyzed in each slide. $*p < 0.05$, $**p < 0.01$ versus their corresponding control. $\#\#p < 0.01$, between MCF-7 and MDA-MB-231 cells.

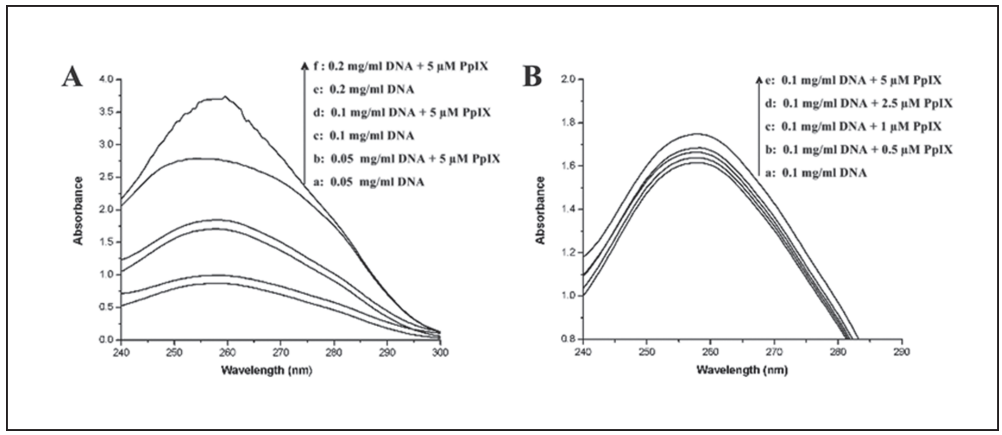

Fig. 6: PpIX induced calf thymus DNA damage. The damage effect on calf thymus DNA was detected by ultraviolet spectrophotometric. The absorbance spectra of calf thymus DNA were recorded. A, different concentration of DNA (0.05 mg/ml, 0.1 mg/ml, 0.2 mg/ml) + 5 μg/ml PpIX, absorbency at 260 nm; B, 0.1 mg/ml DNA + different concentration of PpIX (0.5 μg/ml, 1 μg/ml, 2.5 μg/ml, 5 μg/ml), absorbency at 260 nm.

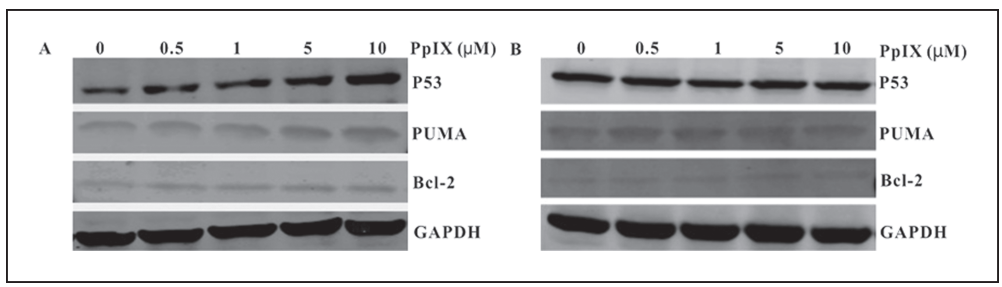

Fig. 7: Western blots staining of P53, PUMA and Bcl-2 in MCF-7(A) and MDA-MB-231(B) cells. GADPH was used a loading control.

after PpIX treatment and that was also in agreement with the P53 protein expression in western blot (Fig. 8B).

3. Discussion

Protoporphyrin IX (PpIX) as an effective hematoporphyrin derivative, widely applied in PDT and SDT cancer research. Our earlier data showed that PpIX mediated SDT (PpIX-SDT) could obviously inhibit the proliferation of sarcoma 180 cells and Ehrlich ascetic tumor cells (Wang et al. 2010a, b). Recently, studies indicated that the PpIX alone can also inhibit Hela cell proliferation (Bednarz et al. 2007), but the potential mechanism was unclear. MCF-7 and MDA-MB-231 are the most widely used breast cancer cell lines to comparatively study cancer biology because of a list of differences, like MCF-7 is an estrogen receptor (ER) positive breast cancer cell line, while MDA-MB-231 is a triple negative breast cancer cell line, and MDA-MB-231 cells express functional caspase-3, whereas MCF-7 cells are caspase-3 deficient (Janicke et al. 1998; Shao et al. 2000; Dampier et al. 2001; Shao and Shen 1999; Monti and Sinha 1994; Yang et al. 1998). In this study, we investigated if the proliferation inhibition effect could generally occurr in MCF-7 and MDA-MB-231 cells, in addition PpIX induced intracellular ROS generation increase, DNA damage, and expression changes of P53 and its downstream.

A number of studies provided evidence that porphyrins preferentially accumulate in tumors because cancerous cells have a generally lower pH (pH∼6.9) compared to healthy cells (pH∼7.4) (Kubát et al. 2004; Tannock and Rotin 1986; Gerweck and Seetharaman 1996). Our data clearly demonstrated that PpIX preferentially accumulated in MCF-7 and MDA-MB-231. After co-incubation with PpIX, the fluorescence intensity of intracellular PpIX was more significant in breast cancer cells than in normal cells. When the concentration of PpIX was up to 10 μM, the mean fluorescence intensities of intracellular PpIX in MCF-7 and MDA-MB-231 cells were 1.74 and 1.55 times higher than that in NIH-3T3 cells. Besides, the PpIX level in MCF-7 was significantly higher than that in MDA-MB-231 cells ($p < 0.05$) (Fig. 1A). The cytotoxic effect on treated cells was in accord with the mean fluorescence intensity of intracellular PpIX (Fig. 2).

Moreover, it has been reported that the peripheral-type benzodiazepine receptor is involved in some way in actions of porphyrins linked with outer mitochondrial membranes (Snyder et al. 1987). The fluorescence captured using laser-scanning confocal microscopy showed that PpIX mostly accumulated in the mitochondria of MCF-7 and MDA-MB-231 cells (Fig. 1B). PpIX accumulated in the mitochondria have great influence on subsequent cell damage, such as MMP (mitochondria membrane potential) loss and ROS generation increased. Emerging evidence has shown that oxidative stress might be one of the major causes that initiate cell death (Song et al. 2011; Yumita et al. 2010), so the generation of intracellular ROS in MCF-7 and MDA-MB-231 was detected.

As displayed in Fig. 3, PpIX led dose dependently increased ROS generation. ROS are generally considered cytotoxic

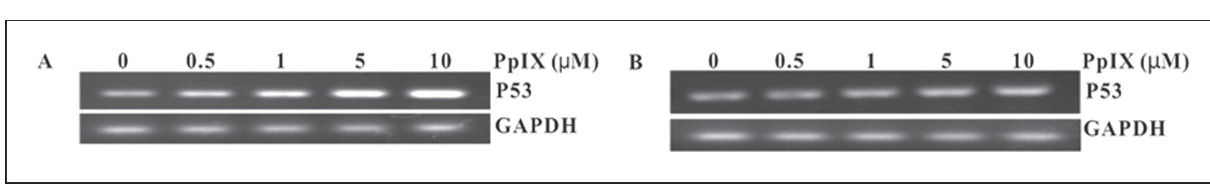

Fig. 8: RT-PCR was used to detect the mRNA expression of p53 in MCF-7(A) and MDA-MB-231(B) cells after different PpIX treatment.

because the radicals can provide oxidative damage to biomolecules such as DNA, proteins and lipids (Park et al. 2005; Valko et al. 2007). To confirm this, we detected DNA damage by DAPI staining and alkaline comet assay. DAPI staining displays nuclear condensation and the nuclear morphology changes, indicating that PpIX induced DNA damage in both cell lines (Fig. 4). Figure 5 shows that after incubation with different concentrations of PpIX for 1 h, the tail length of both MCF-7 and MDA-MB-231 significantly increased compared to control, and the mean levels of comet tail length of MCF-7 is higher than MDA-MB-231 at the same PpIX dose.

To further investigate PpIX caused DNA damage, we examined the interaction between PpIX and calf thymus DNA in a cell-free system. After calf thymus DNA was co-incubated with PpIX, the absorbance of solution was increased (Fig. 6). The absorbance of DNA also increased the positive correlation with the concentration of DNA or PpIX, implying that PpIX destroyed the structure of DNA molecules in *in-vitro* cell free system.

In response to DNA damage, the p53 tumor suppressor gene product was activated leading to the induction of several downstream cellular processes including cell cycle checkpoints, DNA repair or apoptosis. The functions of P53 in the nucleus are repairing damaged DNA, preventing mutations from being passed on to daughter cells. Figure 7 shows that the expression level of P53 and PUMA was increased in MCF-7 but not in MDA-MB-231 cells. After DNA damage had occurred in MCF-7 cells, P53 in nuclear induced enhanced expression of PUMA in MCF-7. When the P53-dependent PUMA expression was induced, PUMA replace P53 in Bcl-xL in cytoplasm (Chipuk et al. 2005) in wt-p53 cell line MCF-7. While mutation of p53 in MDA-MB-231 may have some effects on P53 bind to Bcl-xL, which make PUMA difficult to replace P53 in Bcl-Xl. At the same time, the photosensitizer PpIX binds to wt-p53 in MCF-7 and disrupts the interaction between p53 tumor suppressor protein and its negative regulator HDM2 in cells, p53 accumulates because of disruption of the interaction with HDM2 (Zawacka-Pankau et al. 2007). Normal p53 protein is activated in response to DNA damage, recent discoveries are concerning the regulation of DNA repair processes by p53, such as nucleotide excision repair (NER) and base excision repair (BER) (Smith et al. 1995; Seo et al. 2002). Disturbed/impaired p53 may not have those functions.

In summary, we investigated and compared the anti-tumor activity of PpIX in human breast cancer MCF-7 and MDA-MB-231 cells; the potential mechanism was also evaluated. Due to the different p53 status and in a cell-specific manner, MCF-7 is more sensitive to PpIX than MDA-MB-231 at the same concentration of PpIX, while p53 protein is activated in response to DNA damage in MCF-7 but not MDA-MB-231 after PpIX treatment.

4. Experimental

4.1. Chemicals and reagents

Protoporphyrin IX (PpIX), 3-(4,5-dimethylthiazol-2-yl)-2,5-diphenyltertrazolium bromide tetrazolium (MTT), 4',6-diamidino-2-phenylindole (DAPI) and calf thymus DNA were purchased from Sigma chemical company (St Louis, MO, USA). Mito Tracker Green (MTG) and 2',7'-dichlorodihydrofluorescein-diacetate (DCFH-DA) were supplied by Molecular Probes Inc. (Invitrogen, CA, USA). Antibodies against P53, PUMA were obtained from Cell Signaling Technology (Beverly, USA). Bcl-2 antibody was acquired from Epitomics. Anti-GAPDH monoclonal antibody was supplied by EarthOX Company (San Francisco, CA, USA). Universal RT-PCR kit was purchased from the Dingguo-changsheng biotechnology (Being, China).

4.2. Cell culture

MCF-7, MDA-MB-231 and NIH-3T3 cells were obtained from Shanghai Institutes of Biological Sciences, the Chinese Academy of Sciences. NIH-3T3 cell line was cultured in RPMI-1640 (Gibco, Life Technologies, Inc., USA) and MCF-7 and MDA-MB-231cell lines were cultured in DMEM (Sigma, USA) supplemented with 10 % fetal bovine serum (FBS, Hyclone, USA), 100 IU/ml penicillin, 100 IU/ml streptomycin and 1 mM L-glutamine. Cells were maintained at 37 °C in humidified 5 % CO_2 atmosphere. Cells in the exponential phase of growth were used in each experiment.

4.3. PpIX localization

To investigate the subcellular localization of PpIX in MCF-7 and MDA-MB-231 cells, cells after being loaded with PpIX were then labeled with 10 nM Mito Tracker Green (MTG) at 37 °C for 30 min. After that, cells were washed with PBS for three times, the confocal images of PpIX fluorescence were collected using a 543-nm excitation light from an argon/krypton laser and MTG fluorescence were collected at a wavelength of 488-nm excitation light from the same channel under an inverted confocal laser scanning microscope (TCS SP5 Leica, Wetzlar, Germany). In multi-channel imaging, photomultiplier sensitivities and offsets were set to a level at which bleed through effects from one channel to another were negligible.

4.4. PpIX loading procedure

To make the two cell lines upload sufficient PpIX and because PpIX usually interacts with serum (Brancaleon et al. 2004), different concentrations of PpIX and tumor cells were co-incubated in serum-free DMEM/RPMI-1640 medium for 2 h (this is supported by our previous study) to make sure that PpIX was rapidly enriched in cells, then, the serum was added to ensure the cells cultured in a normal conditions (including 10 % serum) for different incubations as specified in the text.

4.5. Cell viability measurement

A MTT assay was used to monitor the cytotoxicity of PpIX on MCF-7 and MDA-MB-231. Briefly, the treated or untreated cells (100 µl) were added to 96 well culture plates, and cell viability was determined after 24 h incubation by adding 10 µl MTT solution (5 mg/ ml in PBS) to each well and the mixture was incubated for 4 h at 37 °C in a CO_2 incubator. The formed formazan crystals were dissolved in 150 µl DMSO, and the absorbance at 570 nm was recorded using a microplate reader (BIO-TEK ELX800, USA) against the reference value at 630 nm. The cell survival of treated cell samples was then obtained by comparing to the incubated but non-treated control.

4.6. Determination of intracellular ROS

Intracellular reactive oxygen species (ROS) production was studied by measuring the fluorescence intensity of dichlorofluorescein (DCF). 2,7-DCF-diacetate, a non-fluorescent cell-permeant compound, is cleaved by endogenous esterases within the cell and the de-esterified product can be converted into the fluorescent compound DCF upon oxidation by intracellular ROS. At 2 h after different treatment, cells were harvested and stained with 100 nM DCFH-DA for 10 min at 37 °C, washed with PBS and immediately imaged under a fluorescence microscopy.

4.7. Nuclear damage detection

DAPI is a fluorescence probe that binds to natural double stranded DNAs and represents the nuclear morphology. After 6 h incubation post PpIX-loading, cells were stained with 1 µg/ml DAPI for 30 min at 37 °C. The stained cells were washed three times in PBS and observed using a fluorescence microscopy (excitation wavelength was 364 nm, and emission wavelength was 454 nm). The corresponding phase-contrast and fluorescence images were taken.

4.8. Alkaline comet assay

DNA damage was evaluated using the comet assay. Briefly, treated cells were harvested after treatment by different concentrations of PpIX for the indicated incubations, mixed with 0.75 % low melting point agarose, layered onto microscope slides pre-coated with 0.2 % normal melting point agarose, then the slides were submerged in pre-chilled lysis solution (1 % Triton X-100, 2.5 M NaCl, 1 % laurosylsarcosinate and 100 mM Na_2EDTA, 10 mM Tris–HCl, pH 10.5) for 1 h at 4 °C. After soaking with pre-chilled unwinding and electrophoresis buffer (0.3 M NaOH and 1 mM EDTA, pH 13) for 25 min, the slides were subjected to electrophoresis for 25 min at 25 v (300 mA), then stained with 20 µg/ml ethidium bromide (Sigma, USA). Individual cells were viewed using a Nikon E-600 fluorescence microscope. Images were captured with a fluorescence microscope and the comets were analyzed by CASP software. The tail length as a measure of DNA damage in the graphic presentation represents the mean ± SD (standard deviation) of three individual experiments (100 cells from each slide).

4.9. Western blot analysis

Western blots were performed according to standard procedures to assay the levels of proteins including P53, PUMA, and Bcl-2. Briefly, after 24 h incubation post PpIX-loading, cells were harvested and collected by centrifugation, then lysed with RIPA buffer one ice. The protein content of the lysate was measured using the BCA protein assay. Similar amount of protein was analyzed on sodium dodecyl sulfate–polyacrylamide gel electrophoresis gel and transferred onto polyvinylidene fluoride membranes (Millipore). Membranes were then incubated at room temperature for 1 h in blocking buffer (5 % low-fat milk powder in tris-buffered saline-tween 20 (0.05 %) (TBST). The membranes were incubated overnight at 4 °C with primary antibodies. The bound primary antibodies were then tagged with IRDye 680 Conjugated IgG (Li-cor, Biosciences) at room temperature for 1 h. And the infrared fluorescence was detected with the Odyssey infrared imaging system (Li-Cor Bioscience, Lincoln, NE).

4.10. RNA isolation and reverse transcriptase polymerase chain reaction

At 24 h post PpIX-loading, the total cellular RNA was isolated using the HP Total RNA Kit (OMEGA, USA) following the manufacturer's instructions and spectrophotometrically quantified, and the reverse transcriptase–polymerase chain reaction (RT-PCR) was performed with the Bio RT-PCR Kit (Bioer technology, Hang Zhou, China). The reactions were heated at 94 °C for 5 min and then immediately cycled 30 times through a 30 s denaturating step at 94 °C, a 30 s annealing step at 55 °C, and a 30 s extension step at 72 °C. After the cycling procedure, a final 5-minute elongation step at 72 °C was performed. All amplifications were done in the linear range of the assay. The reaction products were separated on a 1.0 % agarose gel, and imaged by a Gel Imaging Analysis system (Beijing Junyi-Dongfang Electrophoresis Instrument Co., Ltd. Beijing, China). The following primers were used: GAPDH (F) 5'-CGCTCTCTGCTCCTCCTGTT-3' and (R) 5'-CCATGG TGTCTGAGCGATGT-3'; p53 (F) 5'-CCTTCCCAGAAAACCTACCAG-3' and (R) 5'-CCAAATACTCCACACGCAAAT-3'.

4.11. UV-Vis spectra measurement the interaction of PpIX with DNA

Calf thymus DNA stock solution was prepared in deionized water and the DNA concentration was 1 mg/ml. Selected the final DNA concentration at 0.1 mg/ml and PpIX concentrations varied from 0.5 μg/ml to 5 μg/ml, the interaction between PpIX and DNA was measured. The UV spectra were recorded in the wavelength of 230-300 nm.

4.12. Statistical analysis

All values were expressed as means ± S.D. Differences among different groups were assessed with one-way ANOVA. Statistical significance was established at a value of $p < 0.01$ and $p < 0.05$.

References

Bednarz N, Zawacka-Pankau J, Kowalska A (2007) Protoporphyrin IX induces apoptosis in HeLa cells prior to photodynamic treatment. Pharmacol Rep 59: 474–479.

Brancaleon L, Magennis SW, Samuel ID, Namdas E, Lesar A, Moseley H (2004) Characterization of the photoproducts of protoporphyrin IX bound to human serum albumin and immunoglobulin G. Biophys Chem 109: 351–360.

Bunz F, Dutriaux A, Lengauer C, Waldman T, Zhou S, Brown JP, Sedivy JM, Kinzler KW, Vogelstein B (1998) Requirement for p53 and p21 to sustain G2 arrest after DNA damage. Science 282: 1497–1501.

Chen X, Wang C, Teng L, Liu Y, Chen X, Yang G, Wang L, Liu H, Liu Z, Zhang D, Zhang Y, Guan H, Li X, Fu C, Zhao B, Yin F, Zhao S (2014) Calcitriol enhances 5-aminolevulinic acid-induced fluorescence and the effect of photodynamic therapy in human glioma. Acta Oncol 53: 405–413.

Chipuk JE, Bouchier-Hayes L, Kuwana T, Newmeyer DD, Green DR (2005) PUMA couples the nuclear and cytoplasmic proapoptotic function of p53. Science 309: 1732–5.

Collado R, Oliver I, Tormos C, Egea M, Miguel A, Cerdá C, Ivars D, Borrego S, Carbonell F, Sáez GT (2012) Early ROS-mediated DNA damage and oxidative stress biomarkers in Monoclonal B Lymphocytosis. Cancer Lett 317: 144–9.

Dampier K, Hudson EA, Howells LM, Manson MM, Walker RA, Gescher A (2001) Differences between human breast cell lines in susceptibility towards growth inhibition by genistein. Br J Cancer 85: 618–624.

Fei P, El-Deiry WS (2003) P53 and radiation responses. Oncogene 22: 5774–5783.

Gerweck LE, Seetharaman K (1996) Cellular pH gradient in tumor vs. normal tissue potential exploitation for the treatment of cancer. Cancer Res 56: 1194–1198.

Hainaut P, Hollstein M (2000) p53 and human cancer: the first ten thousand mutations. Adv Cancer Res 77: 81–137.

Helton ES, Chen X (2007) p53 modulation of the DNA damage response. J Cell Biochem 100: 883–896.

Hinds PW, Finlay CA, Quartin RS, Baker SJ, Fearon ER, Vogelstein B, Levine AJ (1990) Mutant p53 DNA clones from human colon carcinomas cooperate with ras in transforming primary rat cells: a comparison of the hot spot mutant phenotypes. Cell Growth Differ 1: 571–580.

Hollstein M, Sidransky D, Vogelstein B, Harris CC (1991) P53 mutations in human cancers. Science 253: 49–53.

Janicke RU, Sprengart ML, Wati MR, Porter AG (1998) Caspase-3 is required for DNA fragmentation and morphological changes associated with apoptosis. J Biol Chem 273: 9357–9360.

Ji Z, Yang G, Vasovic V, Cunderlikova B, Suo Z, Nesland JM, Peng Q (2006) Subcellular localization pattern of protoporphyrin IX is an important determinant for its photodynamic efficiency of human carcinoma and normal cell lines. J Photochem Photobiol B 84: 213–220.

Jian Yu, Lin Zhang (2005) The transcriptional targets of p53 in apoptosis control. Biochemical and Biophysical Research Communications 331: 851–858.

Kubát P, Lang K, Anzenbacher P Jr (2004) Modulation of porphyrin binding to serum albumin by pH. Biochim Biophys Acta 1670: 40–48.

Kurihara K, Hachimori Y, Shibata K (1963) The hyperchromic effect of organic denaturing reagents on deoxyribonucleic acid. Biochim Biophys Acta 68: 434–445.

Marchenko ND, Zaika A, Moll UM (2000) Death signal-induced localization of p53 protein to mitochondria. A potential role in apoptotic signaling. J Biol Chem 275: 16202–16212.

Monti E, Sinha BK (1994) Antiproliferative effect of genistein and adriamycin against estrogen-dependent and-independent human breast carcinoma cell lines. Anticancer Res 14: 1221–1226.

Nemajerova A, Wolff S, Petrenko O, Moll UM (2005) Viral and cellular oncogenes induce rapid mitochondrial translocation of p53 in primary epithelial and endothelial cells early in apoptosis. FEBS Lett 579: 6079–83.

Park HS, Jin DK, Shin SM, Jang MK, Longo N, Park JW, Bae DS, Bae YS (2005) Impaired generation of reactive oxygen species in leprechaunism through downregulation of Nox4. Diabetes 54: 3175–3181.

Pastorino JG, Simbula G, Gilfor E, Hoek JB, Farber JL (1994) Protoporphyrin IX, an endogenous ligand of the peripheral benzodiazepine receptor, potentiates induction of the mitochondrial permeability transition and the killing of cultured hepatocytes by rotenone. J Biol Chem 269: 31041–31046.

Schneider-Yin X, Kurmanavicieneb A, Rotha M, Roos M, Fedier A, Minder EI, Walt H (2009) Hypericin and 5-aminolevulinic acid-induced protoporphyrin IX induce enhanced phototoxicity in human endometrial cancer cells with non-coherent white light. Photodiagnosis Photodyn Ther 6: 12–18.

Seo YR, Fishel ML, Amundson S, Kelley MR, Smith ML (2002) Implication of p53 in base excision DNA repair: *in vivo* evidence. Oncogene 21: 731–737.

Shao Z, Shen Z (1999) Mechanism of growth inhibition by genistein of human breast carcinoma. Zhonghua Zhongliu Zazhi 21: 325–328.

Shao ZM, Shen ZZ, Fontana JA, Barsky SH (2000) Genistein's "ER dependent and independent" actions are mediated through ER pathways in ER-positive breast carcinoma cell lines. Anticancer Res 20: 2409–2416.

Smith ML, Chen IT, Zhan Q, O'Connor PM, Fornace AJ Jr. (1995) Involvement of the p53 tumor suppressor in repair of u.v.-type DNA damage. Oncogene 10: 1053–1059.

Snyder SH, Verma A, Trifiletti RR (1987) The peripheral-type benzodiazepine receptor: a protein of mitochondrial outer membranes utilizing porphyrins as endogenous ligands. FASEB J 1: 282–288.

Song W, Cui H, Zhang R, Zheng J, Cao W (2011) Apoptosis of SAS cells induced by sonodynamic therapy using 5-aminolevulinic acid sonosensitizer. Anticancer Res 31: 39–45.

Tannock IF, Rotin D (1986) Acid pH in tumors and its potential for therapeutic exploitation. Cancer Res 49: 4373–4384.

Valko M, Leibfritz D, Moncol J, Zheng J, Cao W (2007) Free radicals and antioxidants in normal physiological functions and human disease. Int J Biochem Cell Biol 39: 44–84.

Wang P, Xiao L, Wang X, Li X, Liu Q (2010a) Sonodynamic effects of protoporphyrin IX disodium salt on Ehrlich ascetic tumor cells. Ultrasonics 50: 634–538.

Wang X, Wang P, Tong W, Liu Q (2010b) Comparison of pharmacokinetics, intracellular localizations and sonodynamic efficacy of endogenous and exogenous protoporphyrin IX in sarcoma 180 cells. Ultrasonics 50: 803–810.

Yang X, Stennicke HR, Wang B, Green DR, Jänicke RU, Srinivasan A, Seth P, Salvesen GS, Froelich CJ (1998) Granzyme B mimics apical caspases. Description of a unified pathway for trans-activation of executioner caspase-3 and -7. J Biol Chem 273: 34278–34283.

Yumita N, Okudaira K, Momose Y, Umemura S (2010) Sonodynamically induced apoptosis and active oxygen generation by gallium-porphyrin complex, ATX-70. Cancer Chemother Pharmacol 66: 1071–1078.

Zawacka-Pankau J, Issaeva N, Hossain S, Pramanik A, Selivanova G, Podhajska AJ (2007) Protoporphyrin IX interacts with wild-type p53 protein *in vitro* and induces cell death of human colon cancer cells in a p53-dependent and -independent manner. J Biol Chem 282: 2466–2472.